Fracture Mechanics of Concrete Structures, de Borst et al (eds) © 2001 Swets & Zeitlinger, Lisse, ISBN 90 2651 825 0

Mixed mode fracture of double-edge notched specimens of concrete

J.C.Gálvez
E.T.S. Ingenieros Caminos, Universidad Castilla La Mancha, P. Universidad 4, 13071 Ciudad Real, Spain
D.A.Cendón & M.Elices
Dept. Ciencia de Materiales, E.T.S. Ingenieros Caminos, Universidad Politécnica Madrid, Ciudad Universitaria, 28040 Madrid, Spain

ABSTRACT: The double-edge notched test, suggested by Reinhardt, to explore mixed mode fracture behaviour is analysed. This paper presents detailed experimental data using this novel testing procedure. The tests were performed for three homotetic specimen sizes. Experimental crack trajectories are presented together with the corresponding load-displacement curves. Also, a numerical analysis of the tests was performed. The numerical model is based on the cohesive crack concept and extends it to shear fracture. Numerical results agree quite well with the experimental data. Other experimental set of shear loading fracture of double-edge notched specimens was modelled: the tests from Cedolin and co-workers.

1 INTRODUCTION

Much experimental work has been done to develop testing geometries and procedures for cracks propagating under pure shear fracture mode. The Iosipescu geometry (Iosipescu, 1967) looked very attractive, but after many attemps (Arrea & Ingraffea 1982, Swartz & Taha 1990, Schlangen & Van Mier 1993, Carpinteri et al. 1993, among others), it was concluded that an important governing mode I is always present (Schlangen & Van Mier 1993). Furthermore, Cendón et al. (2000, 2001) showed that under global mixed mode loading, the crack starts from the notch under mixed mode fracture and grows in the direction normal to the maximum principal stress, in local mode I. A noval testing procedure for mode II fracture of concrete was recently proposed by Reinhardt and co-workers (Reinhardt et al. 1997, 1998, Reinhardt & Xu, 2000): the double-edge notched specimen under compression loading at one half specimen.

This paper presents an experimental and numerical analysis of the test proposed by Reinhardt. It is worth to emphasise that two different types of cracks are generated during testing, those generated by the shear stresses in the ligament (shear cracks) and those generated by compression failure (crushing cracks). The mixed mode fracture of concrete was modelled using an improved numerical procedure (Gálvez et al. 1998, Cendón et al. 2001) that reproduces the fracture process of the double-edge notched specimens under compression loading. The experimental load-displacement records and the crack paths were recorded and show very good agreement with measured predictions. The paper ends with an analysis of two sets of experimental data by Reinhardt & Xu (2000) and Cedolin et al. (1999).

2 EXPERIMENTAL PROGRAM

2.1 *Materials and specimens*

A single microconcrete mixture was used to cast the specimens. The microconcrete was composed of Portland cement, siliceous sand as the fine aggregates, and siliceous crushed coarse aggregates of 5 mm maximum size. The material properties were f_c=57MPa, E=38 GPa, f'_t =3.0 MPa and G_F=77 N/m, measured in accordance with ASTM C39, ASTM C469, ASTM C496 and RILEM 50-FMC, respectively.

The dimensions of specimens are detailed in T able 1, the thickness of the specimens was 50 mm. Three specimens were tested in each size. Two symmetric notches were machined on the specimens with a low speed diamond cutting disc. The notches were 2 mm wide with right-angled tip. The ligament length, $2a$, was h, the half of the specimen height, see Figure 1 for details. The support surfaces were ground to avoid spurious displacements due to crushing of the irregularities of the surface and to guarantee the parallelism between both surfaces.

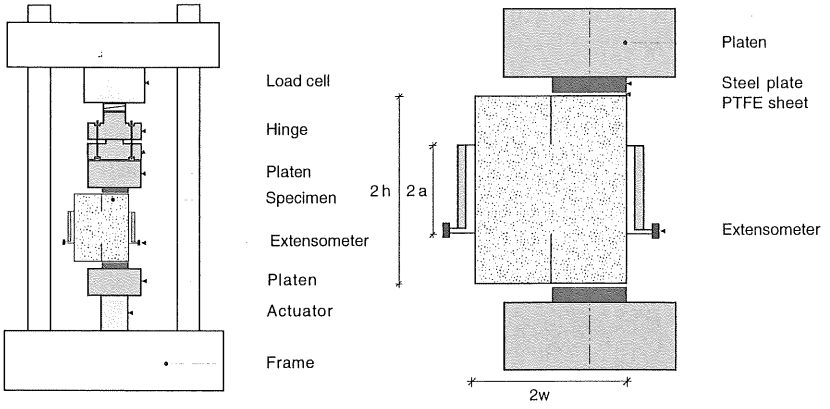

Figure 1. Testing arrangement, geometry and boundary conditions. (a) General view of the testing arrangement. (b) Geometry and instrumentation of the specimen

Table 1: Dimensions of the specimens

Sample	Height, *2h* mm	Length, *2w* mm	Ligament, *2a* mm
H75	75	56.25	37.5
H150	150	112.5	75
H300	300	225.0	150

2.2 *Experimental procedure*

Figure 1 shows the testing arrangement of the double-notched specimens of concrete under compression loading. Two ground and smooth steel plates were put between the machine platens and the upper and bottom faces of the specimen to apply the compression load; the thickness of these steel plates was 10 mm. To eliminate the friction between the steel plate and the concrete a PTFE sheet was introduced, the thickness of the PTFE sheet was 0.2 mm. Between the upper platen and the load cell there was a hinge. Initially a small compression load was applied over the specimen with free rotation hinge; then the hinge was fixed and the whole test was developed with the hinge fixed; in this way it is guaranteed that the compression load is uniformly applied over the whole surface of the steel plates. During the tests the following parameters were recorded: the load P, the displacement of the actuator, the elapsed time and the relative displacement of the points situated at height of the tip notches on the lateral vertical faces of the loaded and unloaded parts of the specimen, see figure 1 for details.

A face of the specimen was covered with a thin film of fluorescein, this product changes his color when the crack opens and the water goes out of the concrete. The map of cracks was plotted along the test and the order of the cracks appearance was established.

The tests were performed in actuator displacement control, at a rate of 0.04 mm/min until 70 percent of the 'oad corresponding with the detection of the first cra :k and 0.02 mm/min until the end of the test.

3 EXPERIMENTAL RESULTS

3.1 *Trajectories of the cracks*

Figure 2 shows the crack trajectories of the double-edge specimens, before the compression failure of the loaded part of the specimen. This figure shows, for two specimen sizes, the crack path of the trajectories in the face of the specimen that was covered with a fluorescein film. All cracks started on the corner of the notch tip that is the most distant of the loaded part of the specimen and grew towards the unloaded unloaded part of the specimen describing a curved path, as it shown in figure 2. The curved path corresponds to a stable growth of the cracks. In some tests a light branch out of the crack was observed.

Figure 3 summarizes a series of consecutive photos showing the sequence of appearance of the cracks on the face of the specimen covered with a thin film of fluoresceine, from the firsts on the notch tip until the compression loading failure of the specimen. This figure shows that two groups of cracks appear along the test: the cracks caused by the shear loading, and the cracks caused by the compression failure. As it observed in the sequence of photos, the cracks caused by the shear loading appear firstly; they are initiated at the corner of the notch tip opposite to the loaded part of the specimen and they grow towards the unloaded part following a curved path, approximately symmetric in the upper and bottom notches. These cracks grow in stable manner until that the compression failure cracks appear. The second photo shows the initiation of a compression crack in the loaded part when the shear cracks have an important length. Since the compression failure governs the failure of the specimen, the shear loading cracks are non completely developed when the specimen colapses, that is the shear cracks do not completely separe the unloaded part of the specimen as a free body. The final photo of the se-

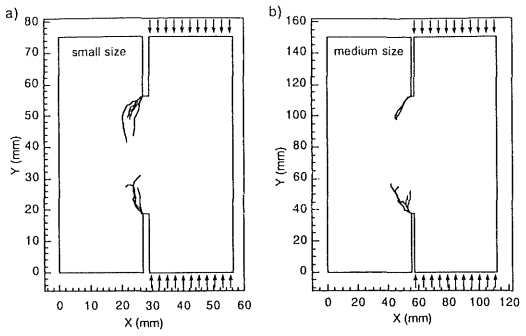

Figure 2. Experimental crack trajectories of double-edge notched specimens of concrete, before the compression failure of the loaded part of specimen. (a) $2h = 75$ mm. (b) $2h = 150$ mm.

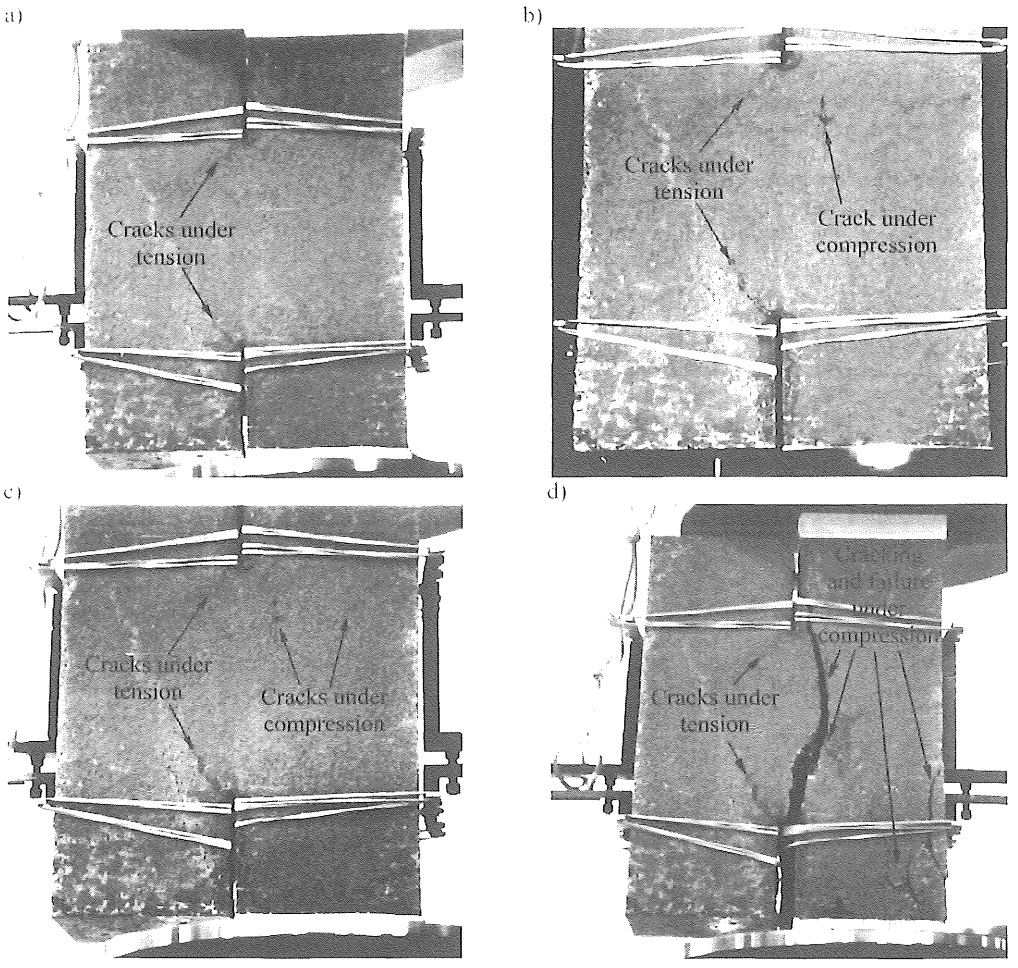

Figure 3. Series of photos showing the sequence of appearance of cracks.

quence, that is the colapsed specimen, shows compression cracks on the loaded part of the specimen and the closed shear cracks. It is worth noting that the cracks caused by the shear fracture process may be no observed with the naked eye because they are closed on the colapsed specimen, and some of the cracks near to the ligament completely opened but caused by the crushing process may be mistaken attributed to the shear fracture process. The thin film of fluoresceine provided to distinguish this two groups of cracks; on the face not covered with fluoresceine some times is very difficult to observe the cracks due to the shear fracture process, specially on the small size specimens.

3.2 *Load-displacement curves*

Figure 4 shows the experimental records load *P versus* relative displacement of the points situated at height of the tip notches on the lateral vertical faces of the loaded and unloaded parts of the specimens. It is worth noting that the scatter band is narrow for both specimen sizes, specially on the loaded side of the specimens. A remanent displacement on the unloaded side is detected in all specimens. The load-displacement curves at the unloaded side show a linear first part following by a curved branch, which return decreasing the displacement with the increasing of the load. The return of the curve is caused by the crack initiation and propagation from the notch, which reduces the load transmitted by the ligament between the loaded to the unloaded parts of the specimen. As it may observed, the lost of linearity of the curves corresponding to the unloaded part is not accompanied by an equivalent lost of linearity of the curves corresponding to the loaded part. The peak load of the test is governed by the compression failure of the loaded part. A small jump on the loaded part curves has been detected for two of the medium size specimen tests.

4 NUMERICAL MODELLING OF THE FRACTURE

The numerical simulation of the mixed mode (I/II) fracture process of concrete proposed in this work is based on the incorporation of the cohesive crack model into a finite element code. The two main stages of the process are the calculation of the crack path, and the incorporation of the cohesive crack model into the crack path, in two computational steps.

4.1 *Numerical prediction of the crack path*

LEFM has proved its worth in predicting the crack path, even of complex trajectories. This was demon-

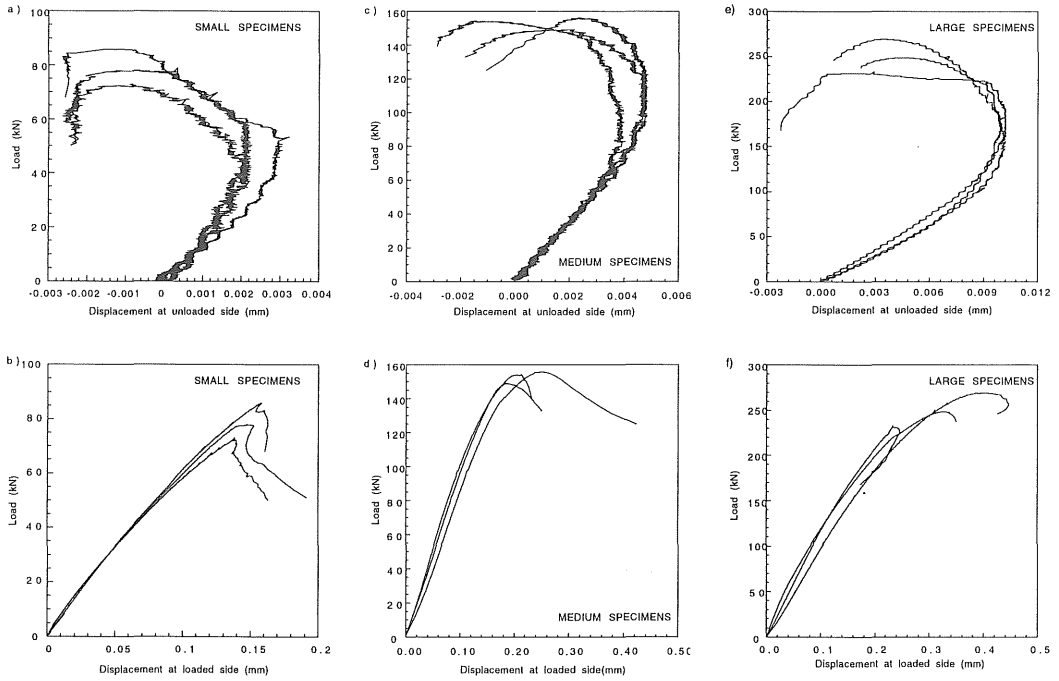

Figure 4. Experimental curves load *P versus* displacement at loaded and unloaded sides of the specimens. (a) and (b) $2h = 75$ mm. (c) and (d) $2h = 150$ mm. (e) and (f) $2h = 300$ mm.

strated in stable tests with brittle materials (Gálvez et al. 1996, Mahajan & Ravi 1989) and extended to quasi-brittle materials (Cendón et al . 2000, Gálvez et al. 1998). In this work, numerical computations use the MTS criterion (Erdogan & Sih 1963), which postulates that the crack grows perpendicularly to the greatest tension. The LEFM finite element code FRANC2D (1994) was used to calculate the crack paths.

4.2 *Cracking surface for mixed mode fracture*

In mixed mode (I and II) fracture, the interaction between normal stress, σ, and tangential stress, τ, should be taken into account. It is assumed that the crack grows when the combination of normal stress, σ, and the tangential stress, τ, reaches a cracking surface $F(\sigma,\tau) = 0$, like a yield surface in classical plasticity. This work assumes the following hyperbolic expression (Cervenka, 1994):

$$F = \tau^2 - 2c\tan\phi_f\left(f_t - \sigma\right) - \tan^2\phi_f\left(\sigma^2 - f_t^2\right) \qquad (1)$$

where: c is the cohesion and, ϕ_f is the friction angle and f_t the traction strength. In accordance with the cohesive approach of Hillerborg et al. (1976), the cracking surface evolves with the opening of the crack , following the softening curves of the traction strength, f_t , and the cohesion, c (figure 5). The softening parameter, u^{ieff}, is the integral norm of the vector the inelastic relative displacements between the crack faces, $\dot{\mathbf{u}}^i$. The inelastic displacement vector is obtained by decomposition of the displacement vector, $\mathbf{u}$, into an elastic part, $\mathbf{u}^e$, and an inelastic part, $\mathbf{u}^i$. It is expressed: $\mathbf{u} = \mathbf{u}^e + \mathbf{u}^i$; $\dot{u}^{ieff} = \left\|\dot{\mathbf{u}}^i\right\| = \left(\dot{u}_x^{i\,2} + \dot{u}_y^{i\,2}\right)^{1/2}$, and the cracking surface $F = F\left(c, f_t\right)$, where $c = c\left(u^{ieff}\right)$ y $f_t = f_t\left(u^{ieff}\right)$. Figure 6 shows the cracking surface and its evolution.

Cendón et al. (2001) have shown that the tangential stresses on the crack are very small in comparison with the traction stresses during the whole tests. The traction stress is quite similar to the traction strength, and a simplification may be done:

$$\sigma + f_t \approx 2f_t \qquad (2)$$

and replacing this value in (1):

$$F = \tau^2 - 2\tan\phi_f\left(c - f_t\tan\phi_f\right)\left(f_t - \sigma\right) \qquad (3)$$

Since the softening parameter for the softening curves of traction strength and cohesion is the same, u^{ieff}, and the adopted form for the curves is equal, it is may be written:

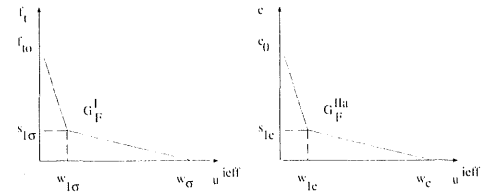

Figure 5. Softening curves. (a) traction strength. (b) cohesion

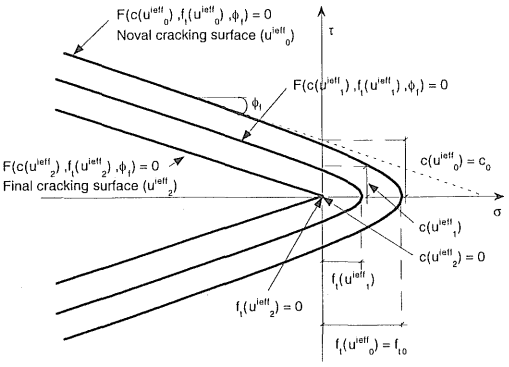

Figure 6. Cracking surface and evolution

$$\frac{c}{f_t} = \frac{c\left(u^{ieff}\right)}{f_t\left(u^{ieff}\right)} = \alpha, \quad \alpha \in \Re \qquad (4)$$

and since friction angle, ϕ_f, is constant:

$$F = \tau^2 - C\,f_t\left(f_t - \sigma\right) \qquad (5)$$

where C is positive real constant. The expression (5) only includes this constant and the traction strength, f_t, which corresponds to the mode I fracture. The traction strength, f_t, evolves according to the softening parameter, u^{ieff}.

The model has been implemented in a finite element code. The classical non associative plasticity formulation has been adopted, based on the "elastic predictor" and the "plastic corrector". Detailed information is shown by Cendón (2001).

5 ANALYSIS OF MIXED MODE FRACTURE TESTS ON DOUBLE-EDGE NOTCHED SPECIMENS

5.1 *Comparison with the experiments by Gálvez and Cendón*

The experimental results shown in the section 2 have been simulated with the above presented numerical procedure. Figure 7 compares the experimental and the numerical predictions of the crack paths of the shear cracks of the three specimen sizes. The nu-

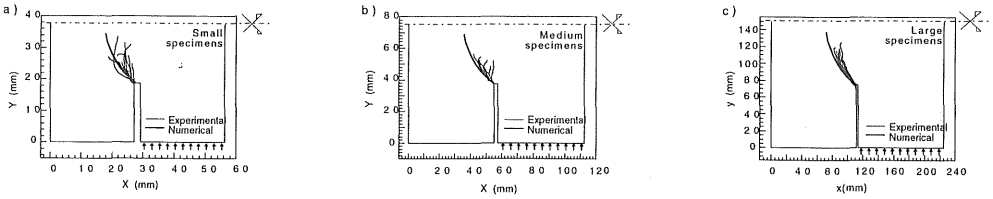

Figure 7. Experimental results and numerical predictions of the crack trajectories of the tests of the authors

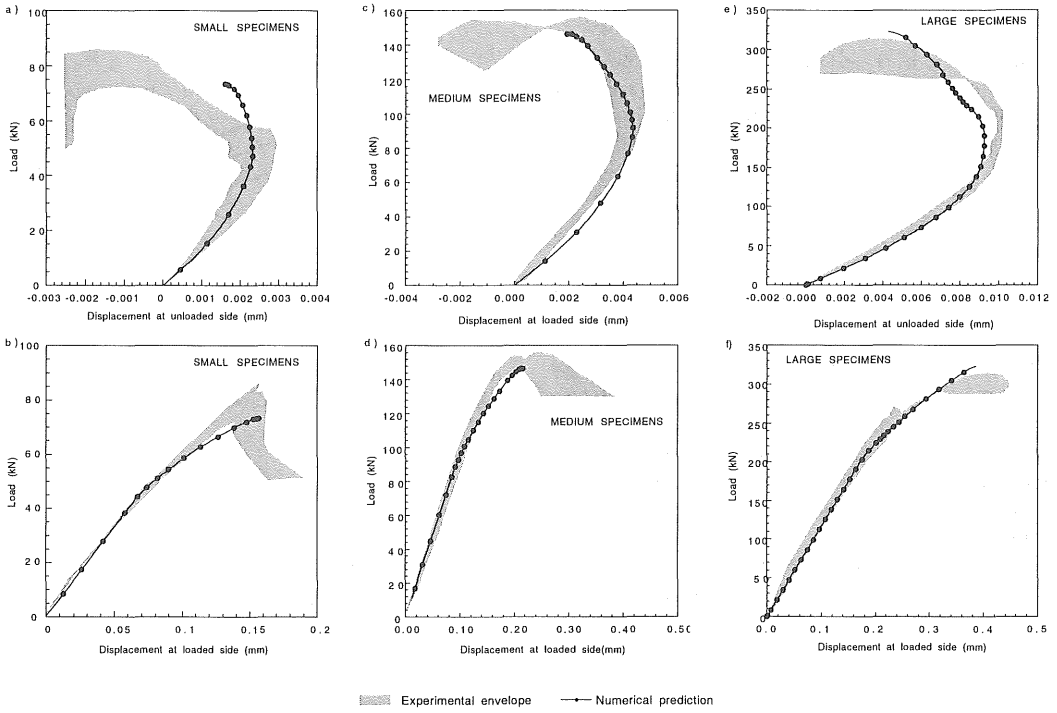

Figure 8. Experimental envelopes and numerical predictions of the load P *versus* displacement at unloaded and loaded sides in the experiments of the authors. (a) and (b) small size ($2h$ = 75 mm). (c) and (d) medium size ($2h$ = 150 mm). (e) and (f) large size ($2h$ = 300 mm)

Table 2: Dimensions of the specimens of the tests in Cedolin et al. (1999)

Sample	Height, $2h$ mm	Length, $2w$ mm	Ligament, $2a$ mm
H60	60	45	30
H120	120	90	60
H240	240	180	120

merical prediction is a good approximation of the crack path.

For the numerical simulation, the experimental measured parameters shown in section 2.1. were used. The kink point of the softening curve (figure 5a) was: $s_{1\sigma}$ = 1.0 MPa, $w_{1\sigma}$ = 0.017 mm, w_{σ} = 0.078 mm, and the parameter C = 1.224. Compression behavior of the concrete was simulated by means of the Menetrey & Willam (1995) model. Figure 8

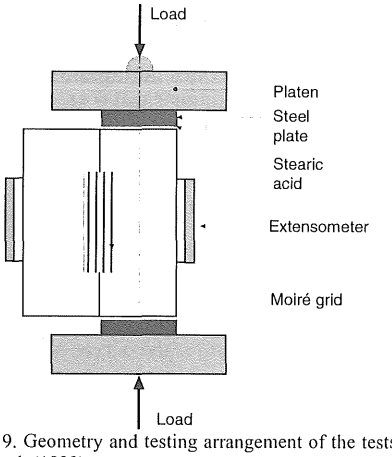

Figure 9. Geometry and testing arrangement of the tests of Cedolin et al. (1999).

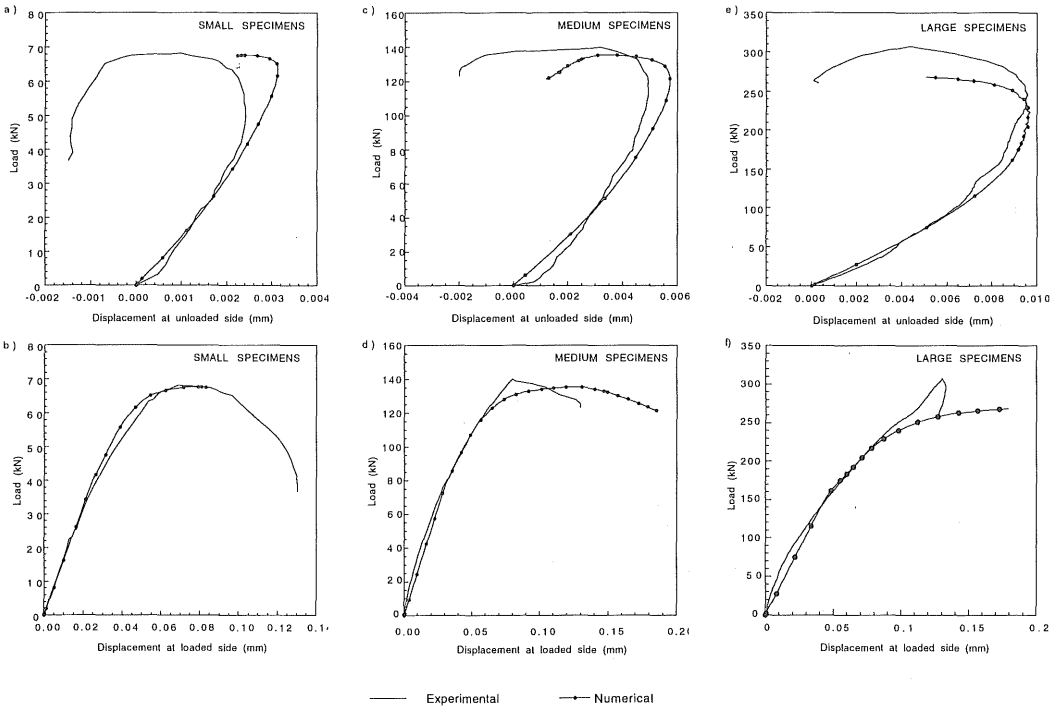

Figure 10. Experimental envelopes and numerical predictions of the load P *versus* displacement at unloaded and loaded sides in the experiments of Cedolin et al. (1999). (a) and (b) small size ($2h$ = 60 mm). (c) and (d) medium size ($2h$ = 120 mm). (e) and (f) large size ($2h$ = 240 mm)

compares the experimental envelope and the numerical prediction of the applied load *versus* displacement recorded by the extensometers placed at the loaded and unloaded half parts of the specimens. The nucleation and growth of the shear cracks, shown in the curves of the unloaded side by the loss of linearity and a marked drawing back, are reproduced by the numerical simulation. The numerical prediction stops at the peak load of the compression side. Numerical modeling of the post peak behavior under compression loading would need an adequate compression model which is beyond the scope of this work. Numerical prediction up to the peak load is good.

5.2 *Comparison with the experiments by Cedolin*

Figure 9 shows the arrangement for the tests developed by Cedolin et al. (1999). The dimensions are detailed in Table 2. Three homothetic specimen sizes were tested. The material properties adopted for the numerical simulation were: f_t = 5.0MPa, E = 30 GPa, G_F=80 N/m and C = 1.2.

Figure 10 shows the experimental results and the numerical prediction of the load versus displacement of the extensometers placed on the loaded and unloaded part of the three sizes ofspecimen. In all cases the numerical prediction adequately fits the experimental records.

6 ACKNOWLEDGEMENTS

The authors gratefully acknowledge financial support for this research provided by Ministerio de Educación y Cultura of Spain under grants PB97-0579 and 1FD97-1641 and Universidad Castilla La Mancha and the Junta de Comunidades de Castilla La Mancha for complementary financial support.

REFERENCES

Arrea, M. & Ingraffea, A. 1982. *Mixed mode crack propagation in mortar and concrete*, Report 81-13, Dpt. Structural Engineering, Cornell University.

Carol, I., Prat, P. & López, M. 1997. Normal/shear cracking model: application to discrte crack analysis. *ASCE Journal of Engineering Mechanics* 123: 765-773.

Carpinteri, A., Valente, S., Ferrar, G. & Melchiorri, G.1993. Is mode II fracture energy a real material property? Computers and Structures 48: 397- 413.

Cedolin, L., GianLuigi, B & Nardello, P..1999, Mode II fracture resistance of concrete, *RILEM Concrete Science and Engineering* 1:1-9.

Cervenka, J. 1994. *Discrete Crack Modelling in Concrete Structures*, Ph. D. Thesis, University of Colorado.

Cendón, D.A., Gálvez, J.C., Elices, M. & Planas, J. 2000. Modelling the fracture of concrete under mixed loading. *International Journal of Fracture* 103: 293-310.

Cendón, D.A., Gálvez, J.C. & Planas, J. 2001. The influence of the mode II in the mixed mode I/II fracture of concrete tests. *International Journal of Fracture* (submitted).

Cendón, D.A. 2001. Ph. D. Thesis, Universidad Politécnica Madrid (in Spanish).

Erdogan, F. & Sih, G.C. 1963. On the crack extension in plates under plane loading and transverse shear, *Journal of Basic Engineering* 85: 519-527.

FRANC2D. 1994. A Two-Dimensional Crack-Propagation Simulator, Version 2.7, Wawryzynek, P. and Ingraffea, A.

Gálvez, J.C., Elices, M., Guinea, G.V. & Planas, J. 1996. Crack trajectories under mixed mode and non-proportional loading. *International Journal of Fracture* 81: 171-193.

Gálvez, J.C., Elices, M., Guinea, G.V. & Planas, J. 1998. Mixed mode fracture of concrete under proportional and nonproportional loading. *InternationalJournal of Fracture* 94: 267-284.

Gálvez, J.C., Cervenka, J., Cendón, D.A. & Saouma, V. 2000. A discrete approach to normal/shear cracking of concrete. *Cement and Concrete Research* (submitted).

Hillerborg, A., Modeer, M. & Petersson, P. 1976. Analysis of crack formation and crack growth by means of fracture mechanics and finite elements. *Cement and Concrete Research* 6, 773-782.

Iosipescu, N. 1967. New accurate procedure for single shear testing of metals. *Journal of Materials* 2: 537-566.

Mahajan, R.V. & Ravi-Chandar, K. 1989. An experimental investigation of mixed-mode fracture. *International Journal of Fracture* 41: 235-252.

Menétrey, Ph. & Willam, K.J. 1995. Triaxial failure criterion for concrete and its generalization. *ACI Structural Journal* 92: 311-318.

Reinhardt, H., Ozbolt, J., Xu, S. & Dinku, A. 1997. Shear of structural concrete members and pure mode II testing. *Advanced Cement Based Materials* 5: 75-85.

Reinhardt, H. & Xu, S. 1998. Experimental determination of K_{IIc} of normal strength concrete. *Materials and Structures* 31: 296-302.

Reinhardt, H. & Xu, S. 2000. A practical testing approach to determine mode II fracture energy of G_{IIF} for concrete. *International Journal of Fracture* 105: 107-125.

Schlangen, E., van Mier, J.G. 1993. Mixed mode fracture propagation: a combined numerical and experimental study. *Fracture and damage of concrete and rock*, 166-175.

Swartz, S.E. & Taha, M. 1990. Mixed mode crack propagation and fracture in concrete. Engineering Fracture Mechanics 35: 137-144.